ARL-TR-8340 ● Apr 2018

US Army Research Laboratory

Propagation of Statistical Noise Through a Two-Qubit Maximum Likelihood Tomography

by Mary Grace M Hager, Daniel E Jones, Brian T Kirby, and Michael Brodsky

NOTICES

Disclaimers

The findings in this report are not to be construed as an official Department of the Army position unless so designated by other authorized documents.

Citation of manufacturer's or trade names does not constitute an official endorsement or approval of the use thereof.

Destroy this report when it is no longer needed. Do not return it to the originator.

ARL-TR-8340 ● APR 2017

US Army Research Laboratory

Propagation of Statistical Noise Through a Two-Qubit Maximum Likelihood Tomography

by Mary Grace M Hager
Cornell University

Daniel E Jones, Brian T Kirby, and Michael Brodsky
Computational and Information Sciences Directorate, ARL

REPORT DOCUMENTATION PAGE

Form Approved
OMB No. 0704-0188

1. REPORT DATE *(DD-MM-YYYY)*	2. REPORT TYPE	3. DATES COVERED (From - To)
April 2018	Technical Report	12/01/2017–2/01/2018

4. TITLE AND SUBTITLE
Propagation of Statistical Noise Through a Two-Qubit Maximum Likelihood Tomography

5a. CONTRACT NUMBER

5b. GRANT NUMBER

5c. PROGRAM ELEMENT NUMBER

6. AUTHOR(S)
Mary Grace M Hager, Daniel E Jones, Brian T Kirby, and Michael Brodsky

5d. PROJECT NUMBER

5e. TASK NUMBER

5f. WORK UNIT NUMBER

7. PERFORMING ORGANIZATION NAME(S) AND ADDRESS(ES)
US Army Research Laboratory
ATTN: RDRL-CIN-T
2800 Powder Mill Road
Adelphi, MD 20783-1138

8. PERFORMING ORGANIZATION REPORT NUMBER
ARL-TR-8340

9. SPONSORING/MONITORING AGENCY NAME(S) AND ADDRESS(ES)

10. SPONSOR/MONITOR'S ACRONYM(S)

11. SPONSOR/MONITOR'S REPORT NUMBER(S)

12. DISTRIBUTION/AVAILABILITY STATEMENT
Approved for public release; distribution is unlimited.

13. SUPPLEMENTARY NOTES

14. ABSTRACT
Quantum state tomography allows for the characterization of unknown quantum states through a series of repeated measurements in different bases of an ensemble of identical states; however, statistical errors prohibit the exact determination of measurement probabilities. In this work, we analyze these statistical counting errors by propagating statistical noise through our tomography system. We perform quantum state tomography measurements for 5 distinct experimental scenarios and digitally add uncorrelated noise to these measurement results. We determine how statistical noise translates into errors in common entanglement measures by comparing the reconstructed density matrices with and without this added noise. Finally, we find minimal statistical variation in the density matrices, concurrences, and purities of the reconstructed states and, thus, conclude that statistical noise is not the dominant cause of variation in performance of our quantum networking testbed.

15. SUBJECT TERMS
quantum networking, quantum tomography, quantum physics, quantum communications, quantum entanglement

16. SECURITY CLASSIFICATION OF:			17. LIMITATION OF ABSTRACT	18. NUMBER OF PAGES	19a. NAME OF RESPONSIBLE PERSON
a. REPORT	b. ABSTRACT	c. THIS PAGE			Brian T Kirby
Unclassified	Unclassified	Unclassified	UU	20	19b. TELEPHONE NUMBER (Include area code) (301) 394-4664

Contents

List of Figures

List of Tables

1. Introduction

Rapid experimental advances in the field of quantum information processing make it essential to understand the methods for verifying and benchmarking quantum states and systems. The process of characterizing unknown quantum states, termed quantum state tomography, consists of a series of repeated measurements in different bases on an ensemble of identical states.[1,2] The statistical properties of these measurement results can then be used to reconstruct the form of the unknown state using a maximum likelihood technique.[1,2] Experimental realizations of quantum state tomography have been implemented in the characterization of 2-photon pure and mixed states,[3–5] 3-qubit Greenberger-Horne-Zeilinger (GHZ)[6] and W states,[7] and qudits in the orbital angular momentum setting.[8,9]

Quantum state tomography is a very general technique that can be used to characterize the quantum states of any number of particles and dimensions. However, this technical report focuses on the 2-qubit scenario, since it corresponds to the quantum states generated in our experimental testbed.[10]

The working principles of 2-qubit state tomography are most easily understood when density matrices are expanded into the Pauli matrices

$$\rho = \frac{1}{4}\sum_{i,j}^{3} S_{i,j}\,\hat{\sigma}_i \otimes \hat{\sigma}_j, \tag{1}$$

where the sigma are the Pauli matrices given by

$$\hat{\sigma}_0 \equiv \begin{pmatrix} 1 & 0 \\ 0 & 1 \end{pmatrix}, \quad \hat{\sigma}_1 \equiv \begin{pmatrix} 0 & 1 \\ 1 & 0 \end{pmatrix}, \quad \hat{\sigma}_2 \equiv \begin{pmatrix} 0 & -i \\ i & 0 \end{pmatrix}, \quad \hat{\sigma}_3 \equiv \begin{pmatrix} 1 & 0 \\ 0 & -1 \end{pmatrix}. \tag{2}$$

The $S_{i,j}$, referred to as the multiple-qubit Stokes parameter, can be expressed in terms of a combination of local projective measurements on each qubit as $S_{i,j} = S_i \otimes S_j$, where each single qubit Stokes parameter is given by

$$S_0 = \langle \varphi_3|\rho|\varphi_3\rangle + \langle \varphi_3^{\perp}|\rho|\varphi_3^{\perp}\rangle, \tag{3}$$

$$S_1 = \langle \varphi_1|\rho|\varphi_1\rangle - \langle \varphi_1^{\perp}|\rho|\varphi_1^{\perp}\rangle, \tag{4}$$

$$S_2 = \langle \varphi_2|\rho|\varphi_2\rangle - \langle \varphi_2^{\perp}|\rho|\varphi_2^{\perp}\rangle, \tag{5}$$

and

$$S_3 = \langle\varphi_3|\rho|\varphi_3\rangle - \langle\varphi_3^{\perp}|\rho|\varphi_3^{\perp}\rangle. \tag{6}$$

The quantum states being projected onto are given by the eigenvectors of the corresponding Pauli matrix

$$|\varphi_1\rangle = \frac{1}{\sqrt{2}}(|H\rangle + |V\rangle), \tag{7}$$

$$|\varphi_2\rangle = \frac{1}{\sqrt{2}}(|H\rangle + i|V\rangle), \tag{8}$$

$$|\varphi_3\rangle = |H\rangle, \tag{9}$$

and their orthogonal compliments. The expected measurement probability of each of these combinations for a given ρ is

$$S_{i,j} = Tr\left[\left(\hat{\sigma}_i \otimes \hat{\sigma}_j\right)\rho\right]. \tag{10}$$

It is clear from the above formalism that an experimentally determined set of joint measurement probabilities can be used to define an unknown quantum state. (For simplicity, we have restricted this discussion to projectors based on the Pauli matrices, but more general state sets can be projected onto, including those which are not orthogonal.)[1,2]

However, the experimental determination of the $S_{i,j}$ requires a large number of measurements to approximate the true probabilities and thus reconstruct the actual density matrix. Consequently, this naïve method is prone to errors for small sample sizes, and can even result in the construction of unphysical density matrices. For this reason, a more sophisticated approach based on maximum likelihood estimation is used to define physical density matrices that are most likely to produce the recorded measurement results.[1,2]

The purpose of this work is to determine how statistical counting errors (which prohibit the exact determination of measurement probabilities) propagate through our tomography system, including the maximum likelihood estimation. Unlike previous research that studies general expressions for error propagation in entanglement metrics,[2] we focus on specific experimental scenarios relevant to our quantum networking testbed. To this end, we perform quantum state tomography measurements for 5 distinct experimental scenarios and digitally add uncorrelated noise to these measurement results. We then compare the reconstructed density matrices found before and after the addition of noise, and determine how this noise translates into errors in common entanglement measures. These results allow us to

establish which quantity variations calculated from reconstructed density matrices are a natural result of statistical noise and which signify other sources of experimental error.

2. Methods

We performed our analysis using quantum state tomography software made freely available by the Kwiat Quantum Information Research Group.[11] This software consists of MATLAB functions capable of performing maximum likelihood tomography, which finds the best estimate of a quantum state given a particular data set. Specifically, we employed the *simple_2q2d_tomography* function, which performs this procedure using the measurement bases, the singles counts at each basis, the coincidence counts, and the accidental counts. We also used several standard entanglement measures implemented in this software through the function *general_bell_fidelity*, which finds the fidelity of an input density matrix with its closest pure maximally entangled state, as well as *concurrence*, *tangle*, and *linear_entropy*, which calculate the measures indicated by their names.

The singles counts (S1 and S2) are the number of events for which one detector (D1 or D2) "clicks" (i.e., detects a photon). Given a photon pair source (such as our entangled photon source (EPS) shown in Fig. 1), entangled photons and noise photons travel in both channels and are registered as singles counts when detected. Coincidence counts (C12) occur when D1 and D2 detect photons at the same time. Since the EPS creates photon pairs in both channels simultaneously, coincidence counts occur when photons generated by the EPS are detected by both D1 and D2. A portion of the coincidence counts result when both detectors happen to detect uncorrelated photons at the same time. These are known as accidental counts (A12) and measure the occurrences where two independent photon streams happen to arrive at detectors D1 and D2 simultaneously.

To understand how errors propagate through the relevant functions, we systematically added noise to different data sets and calculated its affect on the output density matrices and accompanying entanglement metrics. Noise was inserted by adding a random number of counts to the singles (S1, S2) and coincidence (C12) counts of the input data. These random counts were sampled from a normal distribution with a mean of zero and a standard deviation equal to the square root of each individual count. Accidental counts were then calculated based on the simple relation (A12 = S1 × S2 / gates), where the singles counts include the random noise (gates is a user-entered setting which defines how long the detectors measure the EPS output).[10] These values were then used in the

tomography functions outlined above. Statistics were compiled by running each numerical test 100 times.

Many quantum state tomographies were performed for various experimental setups. The primary experimental setups that were tested are denoted as (N1)–(N4), including (N2b), for a total of 5 distinct cases. Each case represents a different combination of pump laser power, number of detection gates, applied polarization-dependent loss (PDL), and applied polarization-mode dispersion (PMD). Figure 1 shows schematic diagrams for each experimental setup.

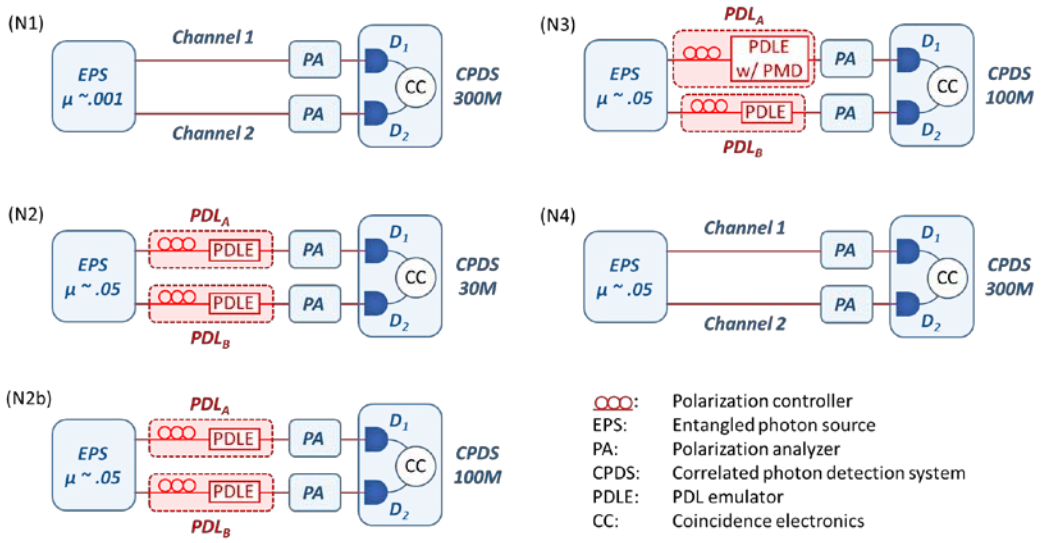

Fig. 1 Experimental setup for each of the five tested cases. Case (N1) depicts a back-to-back setup with low pump power. Cases (N2) and (N2b) depict the setup to perform compensation of PDL in one channel by applying PDL in the other channel. Case (N3) also depicts compensation of PDL; however, channel A includes additional PMD. Case (N4) depicts a back-to-back setup with high pump power.

The (N1) case represents a "back-to-back" measurement with a low pump power setting of 3100 in the Entangled Photon Analyzer (EPA) software (resulting in μ ~ .001) and a long measurement time of 300 million detection gates. A back-to-back measurement is one in which a transmitter (such as our EPS) is directly connected to a receiver/measurement apparatus (such as our polar analyzers and correlated photon detection system) to characterize the behavior of the system when it is not influenced by additional transmission effects. As such, the back-to-back measurement denoted by (N1) has neither applied PDL nor PMD. The (N2) case represents the application of approximately 5 dB PDL to both channels when using a high pump power setting of 3500 in the EPA software (resulting in μ ~ .05) and a short measurement time of 30 million detection gates. The (N2b) case differs from (N2) by only one parameter—a detection time of 100

million gates. (These 2 cases represent experimental demonstrations of PDL compensation.) The (N3) case differs from (N2b) in that the PDL emulator in channel 1 is replaced with a different PDL emulator that also introduces 6.6 ps of PMD. (This case represents experimental demonstration of PDL compensation when subjected to decoherence due to PMD.) Finally, (N4) corresponds to a back-to-back measurement with high power (as with (N2), (N2b), and (N3)) and long measurement time (300 million gates, as with (N1)).

The goal of the tomography analysis is to determine how statistical fluctuations in the measured number of counts affect the calculated density matrix and its concurrence and purity. Specifically, calculation of the density matrix relies on the difference between the number of coincidence counts (for two photons aligned in the same polarization basis) and the accidental counts. This value was therefore analyzed for each of the experimental setups ($C12_{eff} = C12_{max} + C12_{min} - 2 \times A12$). Table 1 includes all of the relevant experimental parameters, measured counts, and calculated results.

Table 1 Relevant experimental parameters (green), measured quantities (orange), and calculated results (blue). The calculated results include the effective coincidences and the noise of relevant density matrix elements and entanglement metrics.

	μ	# gates	S_1	S_2	$C12_{max}$	$C12_{min}$	A12
(N1)	0.001	3.00E+08	9.94E+04	7.31E+04	442	39	29
(N2)	0.050	3.00E+07	3.53E+04	4.72E+04	225	30	56
(N2b)	0.050	1.00E+08	1.15E+05	1.55E+05	786	86	184
(N3)	0.050	1.00E+08	8.31E+04	1.08E+05	407	53	96
(N4)	0.050	3.00E+08	1.59E+06	9.47E+05	31284	5585	5288
	$C12_{eff}$	$\sigma(\rho_{11})$	$\sigma(\rho_{44})$	$\sigma(\rho_{14})$	σ(C)	σ(P)	
(N1)	423	0.0082	0.0089	0.0109	0.0230	0.0223	. . .
(N2)	143	0.0177	0.0108	0.0173	0.0517	0.0416	. . .
(N2b)	504	0.0088	0.0102	0.0149	0.0202	0.0179	. . .
(N3)	268	0.0140	0.0140	0.0212	0.0389	0.0306	. . .
(N4)	26293	0.0013	0.0012	0.0016	0.0032	0.0034	. . .

3. Verification of Data and Results

To verify that all measured coincidence and accidental counts agree with their expected values, a quick loss budget calculation was performed to compare the relative values of S1, S2, C12, and A12. Since A12 is computed directly from the singles counts (S1 and S2), the measured value of A12 was verified with respect to the corresponding S1 and S2 values. The calculated values of these parameters were

found to be in good agreement with the measured values for all 5 experimental cases, as discussed below.

First, we compared the values for all of the high-power cases ((N2)–(N4)). Beginning with the singles counts for (N4), analysis of the loss budget showed agreement between the singles and accidental counts for cases (N2), (N2b), and (N3). To compute the expected values for (N3), we considered the change in counts due to the reduction of the detection time from 300 million gates (for (N4)) to 100 million gates. This reduction in measurement time by a factor of 3 decreases the number of singles counts by a factor of 3 (equivalent to –4.8 dB of loss). Next, we accounted for the addition of 5 dB of PDL in channels 1 and 2, resulting in an additional loss of –2.5 dB in both S1 and S2. Finally, we accounted for the insertion loss of the additional equipment in each channel (the polarization controllers) and the addition of PMD in channel 1. The combined loss due to PMD and the polarization controller in channel 1 was measured and found to be –4.8 dB. Therefore, S1 for the (N3) case should differ from the (N4) value of 1.59E6 by –11.8 dB. This results in an S1 of 1.05E5, which is in good agreement with the measured value of 8.31E4. Channel 2 does not include any added PMD, and the insertion loss of the polarization controller was measured to be –1.25 dB. Therefore, S2 should differ from the (N4) value of 9.47E5 by –8.55 dB. This results in a final expected value of S2 for the (N3) case of 1.33E5, which is also in agreement with the measured value of 1.08E5. Since accidental counts are due to simultaneous occurences of 2 streams of singles counts (A12 = S1 × S2 / gates), the agreement of the expected singles counts with the measured counts reinforces agreement of the accidental counts.

Next, the expected values for the (N2) case were calculated. We first considered the change in counts due to the reduction of the detection time from 300 million to 30 million gates. This reduction in detection time decreases the number of singles counts by a factor of 10 (equivalent to –10 dB of loss). We then account for the addition of 5 dB of PDL in channels 1 and 2. This results in increased loss of –2.5 dB in channels 1 and 2. Finally, we account for the insertion loss of the polarization controllers (there is no PMD for this case). The loss of the polarization controller in channel 1 is –3 dB, resulting in a total decrease in S1 of –15.5 dB. Therefore, the final expected value of S1 for the (N2) case is 4.45E4, which is in agreement with the measured value of 3.53E4. The insertion loss of the polarization controller in channel 2 is –1.25 dB, resulting in a total decrease of –13.75 dB in S2. Therefore, the final expected value of S2 for the (N2) case is 3.98E4, which is also in reasonable agreement with the measured value of 4.72E4.

The (N2b) case analysis differs slightly from the (N2) case—the calculated S1 and S2 values for the (N2) case are multiplied by 3.33 (to account for the increase from 30 million gates ((N2)) to 100 million gates ((N2b)). This results in calculated values of S1 = 1.48E5 and S2 = 1.33E5, which are in agreement with the measured values of 1.15E5 and 1.55E5, respectively. Comparison of the (N2) and (N2b) cases shows that all S1, S2, C12, and A12 values differ only by a factor of 3.33 because of the change in gate number.

Because the number of generated photons (and therefore the values of S1, S2, C12, and A12) is a complicated function of power due to the presence of multiple photon-generating effects[12–15], a "back of the envelope" calculation is inadequate for rapid verification of the relationship between the low-power (N1) and high-power ((N2)–(N4)) measured counts. However, Jones et al.[12,13] show that the relative number of counts between the low and high power cases is in agreement with the expected values. Similarly, this presence of multiple photon-generating effects, as well as the difference in applied PDL and PMD[16–20] among the 5 cases, makes loss budget calculations such as those performed above insufficient to quantitatively analyze the relative magnitude of C12 for each of the 5 cases. Since the coincidence-to-accident ratio (CAR) (C12/A12) provides a good measure of the correlation between two photon streams, we use it to verify the relative magnitude of C12. For example, 2 completely uncorrelated photon streams will have a CAR of 1 because all measured coincidence counts (C12) are merely a result of the statistical coincidence that 1 photon in each channel is detected at the same time (i.e., all measured coincidences are due to accidental coincidences (A12)). A CAR greater than 1 means that the photons are correlated such that they are being generated simultaneously, and more than the expected number of coincidences are being measured for 2 independent, uncorrelated photon streams.

The (N1) case has the greatest CAR (13.9), followed by the (N4) case (5.3), then the (N2), (N2b), and (N3) cases (~2.5)). As expected, the (N1) case has the highest CAR because it is the only case with a low pump power. As the pump power increases, more uncorrelated photons are generated in channels 1 and 2 due to Raman scattering[12,13,21–24] and the relative amount of measured coincidences due to entangled photon pairs decreases. The (N4) case has the second highest CAR due to the lack of applied PDL or PMD. Additional PDL and/or PMD is applied to channels 1 and 2 in the (N2), (N2b), and (N3) cases, resulting in decoherence of the entangled state generated by the EPS. This decreases the amount of coincidences measured due to entangled pairs, which reduces the CAR. The loss budget calculations used to determine S1, S2, and A12 and the qualitative description of the CAR verify the relative magnitudes of all of the S1, S2, C12, and A12 values for each of the 5 cases.

Once all of the measured values (shown in the orange columns in Table 1) were verified, we input the experimental data to the quantum state tomography software discussed in Section 2 (the results are shown in the blue columns of Table 1). The relative results of each case agree with the general trends that would be expected with the addition of random statistical noise; that is, the cases with a greater number of measured counts have lower noise in the calculated density matrix elements (ρ_{11}, ρ_{44}, ρ_{14}), concurrence (C), and purity (P). The very small amount of statistical noise in all of these parameters confirms that statistical noise is not the dominant cause of variation in equipment performance in our quantum networking testbed. For example, we find no greater than approximately 0.05 standard deviation in the concurrence, but we often perform consecutive quantum state tomographies and find a standard deviation of greater than 0.05 in the concurrence. We postulate that the greater variation in our experimental results is largely due to drifts in the behavior of the source, including power drifts and temperature drifts (which change the polarization characteristics of our all-fiber system).

4. Conclusion

Quantum state tomography is a powerful tool for characterizing and benchmarking quantum networking systems. This technical report describes the effects of statistical counting noise on density matrix elements and entanglement measures derived from states reconstructed from maximum-likelihood tomography. Specifically, we have focused on states corresponding to different experimentally relevent scenarios found in our quantum networking testbed. Artificially adding uncorrelated noise proportional to measured counts did not cause the density matrix elements to vary with a standard deviation of greater than approximately 0.05. Additionally, no standard deviations in the concurrence and purity (derived from the density matrices) greater than approximately 0.05 were found in each case and in some cases, were as low as approximately 0.003. From these results, we conclude that statistical counting noise is not a major contributor to variations between runs in our quantum networking testbed. This information will help us analyze system performance as we begin to implement different quantum information processing tasks[25,26] using our quantum networking testbed.

5. References

1. Altepeter JB, Jeffrey ER, Kwiat PG. Photonic state tomography. Advances in Atomic, Molecular, and Optical Physics. 2005;52:105–159.
2. James DFV et al. On the measurement of qubits. Asymptotic Theory Of Quantum Statistical Inference: Selected Papers. 2005;509–538.
3. Peters NA et al. Maximally entangled mixed states: creation and concentration. Physical Review Letters. 2004;92(13):133601.
4. White AG et al. Nonmaximally entangled states: production, characterization, and utilization. Physical Review Letters. 1999;83(16):3103.
5. Wang SX, Moraw P, Reilly DR, Altepeter JB, Kanter GS. Fast measurements of entangled photons. J Lightwave Technol. 2013;31:707–714.
6. Resch KJ, Walther P, Zeilinger A. Full characterization of a three-photon Greenberger-Horne-Zeilinger state using quantum state tomography. Physical Review Letters. 2005;94(7):070402.
7. Mikami H et al. New high-efficiency source of a three-photon W state and its full characterization using quantum state tomography. Physical Review Letters. 2005;95(15):150404.
8. Langford NK et al. Measuring entangled qutrits and their use for quantum bit commitment. Physical Review Letters. 2004;93(5):053601.
9. Molina-Terriza G et al. Triggered qutrits for quantum communication protocols. Physical Review Letters. 2004;92(16):167903.
10. Jones DE, Weninger D, Brodsky M. Setting single photon detectors for use with an entangled photon distribution system. Aberdeen Proving Ground (MD): Army Research Laboratory (US); 2017. Report No.: ARL-TR-8229.
11. Guide to Quantum State Tomography. c2018. Urbana-Champaign (IL): Kwiat Quantum Information Group; [accessed 2017/12/01]. http://research.physics.illinois.edu/QI/Photonics/tomography/.
12. Jones DE, Kirby BT, Brodsky M. In-situ calibration of fiber-optics entangled photon distribution system. In: Photonics Society Summer Topical Meeting Series (SUM); 2017 July 10–12; San Juan (PR). IEEE, 2017. pp. 123–124. doi 10.1109/PHOSST.2017.8012681.

13. Jones DE, Kirby BT, Brodsky M. Joint characterization of two single photon detectors with a fiber-based source of entangled photon pairs. In: Proceedings Frontiers In Optics 2017; 2017 Sep. 18−21; Washington, DC. OSA Publishing; p. JW4A.37. doi:10.1364/FIO.2017.JW4A.37.

14. Alibart O, Fulconis JG, Wong KL, Murdoch SG, Wadsworth WJ, Rarity JG. Photon pair generation using four-wave mixing in a microstructured fibre: theory versus experiment. New J Phys. 2006;8:67.

15. Li X, Ma X, Quan L, Yang L, Cui L, Guo X, Quantum efficiency measurement of single-photon detectors using photon pairs generated in optical fibers. J Opt Soc Am B. 2010;27:1857–1865.

16. Antonelli C et al. Sudden death of entanglement induced by polarization mode dispersion. Phys Rev Lett. 2011;106:080404.

17. Shtaif M, et al. Nonlocal compensation of polarization mode dispersion in the transmission of non-stationary streams of polarization entangled photons. Optics Express. 2011;19:1728–1733.

18. Brodsky M. et al. Loss of polarization entanglement in a fiber-optic system with polarization mode dispersion in one optical path. Opt. Lett. 2011; 36:43–45.

19. Kirby BT, Jones DE, Brodsky M. Local filtering operations on a pair of entangled qubits implemented by a fiber-optic polarization dependent loss emulator. In: Bulletin of the American Physical Society. APS March Meeting 2018; 2018 Mar 5-9; Los Angeles, CA. Ridge (NY): American Physical Society; c2018, Y28.00008.

20. Jones DE, Kirby BT, Brodsky M. Entanglement loss and recovery due to arbitrarily oriented polarization dependent loss for telecom band photon pairs. CLEO: Conference on Lasers and Electro-Optics, Forthcoming 2018 May 13-18, San Jose, CA.

21. Newbury NR. Pump-wavelength dependence of Raman gain in single-mode optical fibers. J Lightwave Technol. 2003;21:3364.

22. Inoue K, Shimizu K. Generation of quantum-correlated photon pairs in optical fiber: Influence of spontaneous Raman scattering. Jpn J Appl Phys. 2004;43:8048.

23. Li X, Voss PL, Chen J, Lee KF, Kumar P. Measurement of co- and cross-polarized Raman spectra in silica fiber for small detunings. Opt Express. 2005;13:2236–2244.

24. Lin Q, Yaman F, Agrawal GP. Photon-pair generation in optical fibers through four-wave mixing: role of Raman scattering and pump polarization. Phys Rev A. 2007;75(023):803.

25. Kirby Brian T et al. Entanglement swapping of two arbitrarily degraded entangled states. Physical Review A. 2016;94(1):012336.

26. Hager MG, Kirby BT, Brodsky M. Modeling quantum teleportation with quantum tools in Python (QuTiP). Adelphi Laboratory Center (MD): Army Research Laboratory (US); 2017. Report. No. ARL-TR-8260.

List of Symbols, Abbreviations, and Acronyms

ARL	US Army Research Laboratory
CAR	coincidence-to-accidental ratio
EPA	Entangled Photon Analyzer
EPS	entangled photon source
PDL	polarization-dependent loss
PMD	polarization-mode dispersion

1 (PDF)	DEFENSE TECHNICAL INFORMATION CTR DTIC OCA
2 (PDF)	DIR ARL IMAL HRA RECORDS MGMT RDRL DCL TECH LIB
1 (PDF)	GOVT PRINTG OFC A MALHOTRA
1 (PDF)	CORNELL UNIVERSITY M HAGER
3 (PDF)	ARL RDRL CIN T D JONES B KIRBY M BRODSKY

INTENTIONALLY LEFT BLANK.